The Exclusion of Glycine Betaine from Anionic Biopolymer Surface: Why Glycine Betaine Is an Effective Osmoprotectant but Also a Compatible Solute†

Daniel J. Felitsky,‡,§,# Jonathan G. Cannon,||,# Michael W. Capp,‡ Jiang Hong,‡ Adam W. Van Wynsberghe,|| Charles F. Anderson,⊥ and M. Thomas Record, Jr.*,‡,⊥

Department of Biochemistry, Program in Biophysics, and Department of Chemistry, University of Wisconsin-Madison, Madison, Wisconsin 53706

Received April 30, 2004; Revised Manuscript Received August 9, 2004

ABSTRACT: Paradoxically, glycine betaine (*N*,*N*,*N*-trimethyl glycine; GB) in vivo is both an effective osmoprotectant (efficient at increasing cytoplasmic osmolality and growth rate) and a compatible solute (without deleterious effects on biopolymer function, including stability and activity). For GB to be an effective osmoprotectant but not greatly affect biopolymer stability, we predict that it must interact very differently with folded protein surface than with that exposed in unfolding. To test this hypothesis, we quantify the preferential interaction of GB with the relatively uncharged surface exposed in unfolding the marginally stable lacI helix-turn-helix (HTH) DNA binding domain using circular dichroism and with the more highly charged surfaces of folded hen egg white lysozyme (HEWL) and bovine serum albumin (BSA) using all-gravimetric vapor pressure osmometry (VPO) and compare these results with results of VPO studies (Hong et al. (2004), *Biochemistry*, *43*, 14744−14758) of the interaction of GB with polyanionic duplex DNA. For these four biopolymer surfaces, we observe that the extent of exclusion of GB per unit of biopolymer surface area increases strongly with increasing fraction of anionic oxygen (protein carboxylate or DNA phosphate) surface. In addition, GB is somewhat more excluded from the surface exposed in unfolding the lacI HTH and from the folded surface of HEWL than expected from their small fraction of anionic surface, consistent with moderate exclusion of GB from polar amide surface, as predicted by the osmophobic model of protein stability (Bolen and Baskakov (2001) *J. Mol. Biol. 310*, 955−963). Strong exclusion of GB from anionic surface explains how it can be both an effective osmoprotectant and a compatible solute; analysis of this exclusion yields a lower bound on the hydration of anionic protein carboxylate surface of two layers of water (≥ 0.22 H_2O $Å^{-2}$).

Cells of many organisms experience a variety of environmental stresses (high external osmolality, desiccation, drought) that reduce the amount of intracellular water (*1*). In response to these water stresses, both prokaryotic and eukaryotic cells transport or synthesize highly soluble, low molecular weight compounds called osmolytes or osmoprotectants that allow the organism to take up and retain cellular water (*1*−*3* and references therein) and resume or sustain normal cellular processes. Osmolytes include *N*-methylated amino acids and amines such as glycine betaine, sarcosine, and trimethylamine-*N*-oxide, amino acids such as glycine, proline, and potassium glutamate, and sugars and polyols such as trehalose and glycerol. Invariably, solutes that are highly effective osmolytes (osmoprotectants) in vivo are preferentially excluded from folded biopolymer surface in vitro (*4*, *5*). Preferential exclusion of the solute is equivalent to preferential hydration; the biopolymer prefers to interact with water rather than with the solute, and as a result, the local concentration of the solute at the biopolymer surface is less than its bulk concentration. Because osmoprotectants are preferentially excluded from folded biopolymer surface, an increase in their concentration increases osmolality efficiently in concentrated biopolymer solutions such as the cell interior (*6*), and indeed, this effect has been proposed to be the basis of their evolutionary selection (*7* and references therein). If excluded from all types of biopolymer surface, these solutes should drive all biopolymer processes in the direction that reduces the exposure of that surface (e.g., folding, binding, self-assembly, aggregation). However, these osmolytes are typically found to be "compatible" solutes that do not greatly affect enzyme activity (*8*−*11*) and do not greatly increase stability of folded proteins and protein complexes (*12*−*15*). Solutes that do not affect biopolymer stability are neither preferentially accumulated near nor excluded from the biopolymer surface that is exposed in unfolding. In this paper, we explain how these observations can be reconciled.

Glycine betaine (*N*,*N*,*N*-trimethylglycine; GB)[1] is one of the most widespread osmolytes, found in bacteria, halophilic archaebacteria, marine invertebrates, plants, and kidneys of some mammalian species (*1*, *16*−*21*). In *Escherichia coli*,

† This work was supported by NIH Grant GM 47022. D.J.F. acknowledges support from an NSF Predoctoral Fellowship and a Wharton Fellowship. J.G.C. acknowledges support of the NIH Molecular Biophysics Training Grant.

* Corresponding author. Mailing address: 433 Babcock Dr., Madison, Wisconsin 53706. E-mail: record@biochem.wisc.edu. Phone: (608) 262-5332. Fax: (608) 262-3453.

‡ Department of Biochemistry.

§ Current address: The Scripps Research Institute, La Jolla, California 92037.

# These authors contributed equally to this work.

|| Program in Biophysics.

⊥ Department of Chemistry.

10.1021/bi049115w CCC: $27.50
Published on Web 10/30/2004

GB is the most efficient osmoprotectant characterized to date (*2*, *6*). In vitro, GB is preferentially excluded from folded bovine serum albumin and lysozyme (*4*, *5*, *22*) and increases the thermal stability of proteins modestly (*12*, *14*, *15*, *22*), indicating that it is also preferentially excluded from the surface exposed upon unfolding. Bolen and co-workers (*23*−*26*) proposed that exclusion of GB and other osmolytes from the peptide group of proteins (the "osmophobic effect") explains their ability to stabilize globular proteins. Quantitative comparisons of preferential interactions of GB with various folded and unfolded biopolymer surfaces have not previously been attempted. This information is needed to predict or interpret effects of GB concentration on biopolymer processes in terms of changes in the area and composition of solvent-accessible biopolymer surface.

In this study, preferential interaction coefficients, Γ_{μ_3}, characterizing the interaction of GB with the surface exposed upon unfolding the marginally stable lacI helix-turn-helix (HTH) domain are obtained by measuring the dependence of the observed equilibrium constant (K_{obs}) for unfolding on GB concentration. Preferential interaction coefficients characterizing the interaction of GB with the folded protein surface of bovine serum albumin (BSA) and hen egg white lysozyme (HEWL) are obtained as a function of GB concentration using vapor pressure osmometry (VPO). Analysis of Γ_{μ_3} using the solute partitioning model (*5*, *27*, *28*) quantifies the average local concentration deficit of GB at each protein surface as a function of GB concentration. In a companion study (*65*), VPO is used to quantify the preferential interactions of GB and of urea with duplex (double-stranded) DNA surface. The thermodynamics of interaction of GB with the protein surface exposed upon unfolding and with folded biopolymer surface provide quantitative support for a model in which GB is strongly excluded from hydrated anionic surface and moderately excluded from hydrated polar amide surface. This model predicts that anionic carboxylate surfaces of proteins are hydrated by at least two layers of water. Hong et al. (*65*) analyze the preferential interactions of urea with protein and DNA surfaces and conclude that urea is moderately accumulated in the vicinity of polar amide surfaces of proteins and amide-like surfaces of DNA bases and is neither accumulated nor significantly excluded from anionic protein and DNA surface.

EXPERIMENTAL PROCEDURES

Materials. Betaine monohydrate (GB, >99% pure, FW 135.2) and certified ACS grade NaCl (FW 58.44) were obtained from Sigma-Aldrich (St. Louis, MO). Anhydrous K_2HPO_4 (99.7% pure, FW 174.18) and certified ACS grade KCl (FW 74.56) were obtained from Fisher Scientific (Pittsburgh, PA). All were used without further purification. Bovine serum albumin (BSA, catalog no. A6918) and hen egg white lysozyme (HEWL, catalog no. L6876) were obtained from Sigma. Expression and purification of the 62-residue lacI DNA-binding domain, composed of the 51 residue HTH and an unstructured 11 residue connector ("hinge helix") were performed as described previously (*29*, *30*). Barnstead E-Pure treated (18+ MOhm), house deionized water was used in all experiments.

Circular Dichroism Studies of LacI HTH Unfolding. LacI HTH samples were prepared by dialysis against 25 mM K_2HPO_4, pH 7.3 (adjusted using HCl), and adjusted to the desired GB concentration by volumetric addition of buffered GB stock solutions (2.0−4.0 M) using the procedure of Felitsky and Record (*30*). The thermal unfolding transition of lacI HTH was monitored using circular dichroism at 236 nm, and the data were fitted to a two-state equilibrium unfolding model (*30*). Pre- and post-transition ellipticities, which correspond to the signals from the folded and unfolded states of the protein, respectively, were fit as linear functions of temperature to calculate fractional extents of unfolding at constant GB concentration. (Slopes of these linear baselines, where individually determined, were not significantly dependent on GB concentration, and therefore data for the unfolded state at low GB concentration was used to establish the high-temperature baseline at high GB concentration.) Because lacI HTH concentration is dilute, molal GB concentrations (m_3) were calculated from molar concentrations (C_3) at 25 °C using the two component equation $m_3 \cong C_3 m_1^\bullet \bar{V}_1^\bullet/(1 - C_3\bar{V}_3)$, where 1 and 3 denote water and GB, respectively, and where $\bar{V}_1^\bullet = 0.01806$ L mol^{-1} and $\bar{V}_3$(25 °C) = 0.0982 L mol^{-1} (*5*). $\bar{V}_3$ decreases from 0.0985 to 0.0980 from 0 to 4 M GB (data not shown); incorporating this variability in partial molar volume has a negligible effect on calculated molal concentrations (<0.5% at all concentrations). Molal scale activity coefficients up to 4.94 *m* GB were calculated by interpolation of isopiestic distillation data (*31*), using a cubic polynomial fit (*32*). Above 4.94 *m* GB, activity coefficients were estimated by extrapolation of this cubic polynomial fit.

Vapor Pressure Osmometry (VPO) to Quantify GB−*Protein Preferential Interactions.* "Salt-free" BSA, pH 7, was prepared as described previously (*5*). HEWL, initially at concentrations of 300−370 mg/mL and pH 6.5, was dialyzed in 3500 MWCO dialysis tubing (Spectrum) against three separate 2 L volumes of successively lower salt concentrations (final salt concentrations of either 5 mM NaCl with 2.5 mM HEPES or 25 mM KCl, both at pH 6.5). The solutions were concentrated by vacuum centrifugation, and the new volumes were used to calculate final buffer and salt concentrations. Protein concentrations were determined from absorbance readings at 280 nm using extinction coefficients of $\epsilon^{1\%}_{280nm} = 6.5$ for BSA and $\epsilon^{1\%}_{280nm} = 26.4$ for lysozyme. All-gravimetric serial dilutions of the concentrated protein solutions were used to minimize experimental uncertainties. All other solutions for osmometric studies were prepared gravimetrically in a manner analogous to that of Hong et al. (*65*), which significantly reduces the potential for systematic errors in calculating molal GB concentrations (when GB solutions are mixed with concentrated protein solutions) relative to previous procedures with one gravimetrically calibrated volumetric step (*5*, *33*). Two vapor pressure osmometers were used as described previously (*5*, *33*−*35*). A majority of measurements were made on the VAPRO 5520 osmometer (Wescor, Logan, UT) at ambient temperature (23−25 °C). A minority were made with the VAPRO 5500 at 37 °C. No systematic difference was observed between the results obtained with the two osmometers.

[1] Abbreviations: lacI DBD, lac repressor DNA-binding domain; HTH, helix-turn-helix domain; CD, circular dichroism; GB, glycine betaine (*N*,*N*,*N*-trimethyl glycine).

Data Analysis. From VPO data, we calculate the difference, Δ_{23}Osm, between the osmolality Osm(m_2,m_3) of a three-component solution (containing water, biopolymer, and solute, denoted as components 1, 2, and 3, respectively) and the sum of osmolalities of the two corresponding binary solutions Osm(m_2) + Osm(m_3) (where the molality of the solute in each binary solution is identical to its molality in the ternary solution):

$$\Delta_{23}\mathrm{Osm} \equiv \mathrm{Osm}(m_2,m_3) - [\mathrm{Osm}(m_2) + \mathrm{Osm}(m_3)] \quad (1)$$

To an excellent approximation under the conditions examined in the present study (*34*, *36*, Anderson et al., manuscript in preparation), at a given m_2, m_3, and T, the value of Δ_{23}Osm is proportional to the derivative of the biopolymer chemical potential (μ_2) with respect to the GB molality, designated μ_{23}:

$$\frac{\Delta_{23}\mathrm{Osm}}{m_2 m_3} \cong \frac{1}{RT}\left(\frac{\partial \mu_2}{\partial m_3}\right)_{T,P,m_2} \equiv \frac{\mu_{23}}{RT} = \left(\frac{\partial \ln \gamma_2}{\partial m_3}\right)_{T,P,m_2} \quad (2)$$

where γ_2 is the molal scale activity coefficient of the biopolymer.

The extent of exclusion or accumulation of GB near the protein surface is quantified by the preferential interaction coefficient:

$$\Gamma_{\mu_3} = \frac{\mu_{23}}{\mu_{33}} \quad (3)$$

where $\mu_{33} \equiv (\partial\mu_3/\partial m_3)_{T,P,m_2}$. At specified m_2 and m_3, the derivative μ_{23} is obtained from Δ_{23}Osm (eq 2) and μ_{33} is obtained from Δ_{23}Osm and $(\partial\mathrm{Osm}/\partial m_3)_{m_2}$ using the ternary Gibbs−Duhem relationship:

$$\mu_{33} = \frac{m_1^{\bullet}\mu_{13} + m_2\mu_{23}}{m_3} = \frac{RT}{m_3}\left(\frac{\partial \mathrm{Osm}}{\partial m_3}\right)_{m_2} - \frac{RT\Delta_{23}\mathrm{Osm}}{m_3^{\,2}} \quad (4)$$

The relationship between osmolality and water chemical potential, $\mathrm{Osm} = -m_1^{\bullet}(\mu_1 - \mu_1^{\bullet})/(RT)$, and eqs 1 and 2 are used in obtaining the second equality in eq 4. Uncertainty in Γ_{μ_3} was propagated by standard methods (*37*).

VPO data on HEWL−salt−GB four component solutions, in which GB concentration was varied in a series at constant molal concentrations of HEWL and salt, were analyzed using a four-component analogue of eq 1:

$$\Delta_{[2,4]3}\mathrm{Osm} \cong \mathrm{Osm}(m_2,m_3,m_4) - [\mathrm{Osm}(m_2,m_4) + \mathrm{Osm}(m_3)] \quad (5)$$

Equation 5 treats HEWL and salt as a composite component (Anderson et al., manuscript in preparation) and assumes that the contributions of GB (component 3) and salt (component 4) to osmolality of a three-component GB−salt solution are additive: (Osm(m_3,m_4) ≅ Osm(m_3) + Osm(m_4)). Comparative applications of eq 5 and of a more general four-component analysis (*65*) to VPO data on interactions of GB, salt, and DNA indicate that the approximations introduced in eq 5 for interactions of GB and salt should be reliable at the low salt concentrations (∼12−20 m*m*) of four of our five series of HEWL experiments. A fifth series of VPO measurements on HEWL at $m_4 \cong 120$ m*m* agrees within the uncertainty of the four HEWL experiments at lower salt molality (as demonstrated by Figures 4 and 5).

To calculate osmolality differences using eq 1 for GB−BSA interactions or eq 5 for GB−HEWL interactions, Osm(m_2,m_3) for BSA or Osm(m_2,m_3,m_4) for HEWL was measured directly. Osm(m_3) was interpolated from a quadratic fit to eight GB−water data sets, including a set of isopiestic distillation data (*31*). Extrapolation to $m_3 = 0$ of quadratic fits to osmolality of each GB−protein data set (at constant m_2 or m_2 and m_4) yielded Osm(m_2) or Osm(m_2,m_4). Data up to 2 *m* GB from five of six GB−BSA data sets were included in the analysis. The average value of μ_{23} for the sixth data set was 2.0 standard deviations from the average of the six sets, while the other five were all within 0.8 SD. All five sets of GB−HEWL data were included in the analysis to determine Γ_{μ_3} by applying eqs 2−5.

Significant improvements in methodology have greatly increased the precision and accuracy of VPO-based determinations of Γ_{μ_3} for GB−protein interactions as compared with some of our earlier published results. First, and foremost, we now use only gravimetric methods to prepare solutions and determine solution composition. Previously, delivery of concentrated BSA solutions from gravimetrically calibrated micropipets in serial dilutions to determine BSA concentration and in preparing samples for VPO led to a systematic underestimate of BSA concentration and consequent underestimates of GB and proline concentrations in measurements of GB and proline interactions with BSA (*5*). Revised values for GB−BSA interactions are reported here. Revised proline−BSA results will be reported subsequently. Preliminary results for interactions of other solutes with BSA indicate much smaller differences between previously reported gravimetrically calibrated values and new all-gravimetric results than for GB and proline (Cannon, Capp et al., manuscript in preparation). Second, use of the ΔOsm analysis (as applied in ref *34*) to determine μ_{23} and Γ_{μ_3} (eqs 1−5 above) eliminates the need to differentiate a polynomial fit of the solute−biopolymer osmolality data, as was previously required (*5*, *33*). Osmolality measurements are here multiplied by a factor of 1.015 to correct for the difference between the stated osmolality of Wescor standard NaCl solutions used in VPO and currently accepted literature standards (*38*) as described by previously (*34*).

Solute Partitioning Local−Bulk Model. The local−bulk solute partitioning model (*5*, *27*, *28*) was used to analyze preferential interaction coefficients, Γ_{μ_3}, characterizing the accumulation or exclusion of solutes from the local water of hydration of protein or nucleic acid surface. At low solute concentrations (*5*, *35*, *39*),

$$\frac{\Gamma_{\mu_3}}{m_3^{\mathrm{bulk}}\mathrm{ASA}} \approx \frac{(K_P^{\circ} - 1)b_1^{\circ}}{m_1^{\bullet}} \quad (6)$$

where K_P° is the low solute concentration limiting value of the local−bulk partition coefficient of the solute ($K_P^{\circ} \equiv (m_3^{\mathrm{loc}}/m_3^{\mathrm{bulk}}))^{\circ}$, b_1° is the amount of water per Å^2 of protein surface area in the thermodynamically defined local domain in the absence of small solute, m_3^{bulk} is the bulk solute concentration (molal, designated as m_3^* in eq 4 of ref *5*), ASA is the water accessible surface area (see below), and $m_1^{\bullet} = 55.5$ mol of H_2O/kg of H_2O. Equation 6 was derived

Table 1: Accessible Surface Areas (ASA) and Surface Compositions of Biopolymers

biopolymer surface	ASA (10^3 Å^2)	% composition of ASA[a] charged (−/+)	polar amide	nonpolar
unfolding lacI HTH (ASA^{Δ})[c]	3.5	2.2/4.1	16.0	72.5
folded HEWL	6.5	4.5/16.9	27.3	45.9
folded BSA	27.8	16.4/13.1	14.6	52.9
duplex monosomal calf thymus DNA	0.17[b]	44/0.0	2.5	38

[a] Defined as in Experimental Procedures. [b] Per nucleotide; from Hong et al. (*65*). [c] ASA^{Δ} is the ASA exposed upon unfolding ($ASA^{\Delta} \equiv ASA_{unfolded} - ASA_{folded}$).

for the dialysis preferential interaction coefficient, Γ_{μ_1,μ_3} (*40*), which, to an excellent approximation, is equal to Γ_{μ_3} for the systems and conditions investigated here (*41*). $\Gamma_{\mu_3}/m_3^{bulk}$ is reported as the average of slopes of Γ_{μ_3} vs m_3^{bulk} determined by linear fits of each relevant data set with the intercept fixed at zero (the limit required by mixing entropy contributions for systems of the type considered here (*42*)). Error is reported as 1 SD of the average (Table 3). In CD experiments at low m_2, m_3^{bulk} does not differ significantly from m_3; values of $\Gamma_{\mu_3}/m_3^{bulk}$ and Γ_{μ_3}/m_3 differ by less than 4% for the VPO experiments reported here.

Surface Area Calculations. A summary of surface area calculations is provided in Table 1. The accessible surface areas (ASA) of the folded state and extended β-chain model of the unfolded state of lacI HTH were calculated as described previously (*32*) using the file 1CJG.PDB in the Protein Data Bank (www.rcsb.org). The ASA reported for the surface exposed in unfolding lacI HTH, designated ASA^{Δ}, is defined as the difference in ASA between the extended β-chain model of the unfolded state and the folded state. Use of an alternative extended (polyproline II) model (*43*) for the unfolded state of lacI HTH does not affect the calculated ASA^{Δ} significantly. Accessible surface areas for BSA (modeled as HSA) and HEWL were calculated from the pdb files 1BM0.PDB and 5LYM.PDB (average of two structures). (Our previous calculation for a BSA precursor (*5*) yielded a surface area 4% larger than the value for BSA.) Protein anionic ASA is defined as the ASA of oxygen atoms in aspartate, glutamate, and the C-terminal carboxylate groups. Protein cationic surface is defined as ASA of nitrogens in the guanidinium group of arginine, the quaternary ammonium group of lysine, the imidazole group of histidine, and the N-terminal amino group. Polar amide surface of proteins is defined as the ASA of N and O atoms of backbone amide groups and side chain amides of asparagine and glutamine. The ASA of native DNA was calculated as described elsewhere (*65*). DNA anionic surface is defined as the ASA of the two partially double bonded oxygens of each phosphate group, and DNA "amide" surface is defined as the ASA of those nitrogen and carbonyl oxygens found in amide-like functional groups of G, C, and T bases (*65*).

RESULTS

Effects of GB on the Transition Temperature and Enthalpy of Unfolding of lacI HTH. Thermal unfolding experiments with lacI HTH were performed at GB concentrations between 0.0 and 4.0 M at 0.25 M increments and monitored by circular dichroism spectroscopy at 236 nm. The strong UV absorbance of GB solutions at lower wavelengths prevents CD experiments at 222 nm, the wavelength typically used in studies of unfolding of α-helical proteins. In the absence of GB, we find that the normalized thermal unfolding transition of lacI HTH at 236 nm agrees within experimental uncertainty with that reported at 222 nm (*30*). Unfolding transitions were in all cases greater than 95% reversible, as judged by the extent of signal recovery after cooling the heated samples back to 4 °C. A representative series of thermal unfolding data at 1 M intervals of GB concentration (selected from our larger data set; Table 2) is shown in Figure 1. With each 1 M increase in GB concentration, the cooperative unfolding transition shifts to higher temperature by ∼7−8 °C and the transition breadth (defined as $dT/d\theta$ at T_m) decreases by ∼2 °C, from ∼29 °C in the absence of GB to ∼22 °C at 4 M GB. Individual unfolding transitions are accurately fitted by a completely cooperative two-state equilibrium unfolding model using linear empirical pre- and post-transition baselines. Values for the midpoint transition temperature T_m (where $\Delta G^\circ_{obs} = 0$), $\Delta H^\circ_{obs}(T_m)$, and $\Delta C^\circ_{p,obs}$ obtained from these fits are compiled in Table 2.

In the absence of GB, lacI HTH is marginally stable: $T_m = 45.8 \pm 0.2$ °C at 50 mM K^+ (as potassium phosphate; pH 7.3). At this temperature, $\Delta H^\circ_{obs} = 27.8 \pm 2.1$ kcal mol^{-1}; the relatively small transition enthalpy results in a relatively broad, though completely cooperative, thermal transition, so unfolding can be investigated over a wide range of temperatures. Indeed even at the temperature of maximum stability ($T_S = 8$ °C) only ∼94% of the population of lacI HTH molecules are in the folded state (*30*), as indicated by the less negative values of $[\theta]_{236}$ below 20 °C for unfolding in the absence of GB compared to the presence of 1−4 M GB (see Figure 1). As the concentration of GB increases, both T_m and $\Delta H^\circ_{obs}(T_m)$ increase; as a consequence of the increase in the transition enthalpy, the transition breadth decreases. At 4 M GB, $T_m = 73.0 \pm 0.2$ °C and $\Delta H^\circ_{obs}(T_m) = 42.7 \pm 5.2$ kcal mol^{-1}. Values of $\Delta H^\circ_{obs}(T_m)$ and T_m in Table 2 are quite accurately determined (average uncertainty of ±0.2 °C in T_m and ±8% in $\Delta H^\circ_{obs}(T_m)$), but at all GB concentrations, only an estimate of $\Delta C^\circ_{p,obs}$ is obtained (0.65 ± 0.21 kcal mol^{-1} K^{-1}). Analogous studies of the effect of urea concentration on the stability of the lacI HTH (*30*), in which the temperature range of the data included the characteristic temperatures T_H and T_S where ln K_{obs} and ΔG°_{obs} exhibit extrema, yielded a more accurate determination of $\Delta C^\circ_{p,obs}$ (0.63 ± 0.05 kcal mol^{-1} K^{-1}).

Isothermal GB-Induced Folding of lacI HTH. To examine the effects of GB on the folding equilibrium of the marginally stable lacI HTH, all ellipticity data for thermal unfolding transitions (including the subset shown in Figure 1) were analyzed using linear baselines (see Experimental Procedures) to obtain the fraction of unfolded protein as a function of GB concentration at each temperature investigated. These data are plotted in Figure 2 as isothermal GB-induced folding transitions at different temperatures from 23.2 to 94.9 °C. Fits shown to these transitions in Figure 2 were obtained for a two-state (completely cooperative) equilibrium folding process assuming a GB concentration-independent *m*-value at each temperature. The GB *m*-value is defined by analogy with denaturants as the negative of the slope of a linear plot

Table 2: Thermodynamic Parameters for Two-State Equilibrium Unfolding of LacI HTH

C_3 (25 °C)	m_3	a_3 (25 °C)	T_m (°C)	$\Delta H^\circ_{obs}(T_m)$ (kcal mol^{-1})	$\Delta S^\circ_{obs}(T_m)$ (cal mol^{-1} K^{-1})	$\Delta C^\circ_{p,obs}$ (kcal mol^{-1} K^{-1})
0.00	0.00	0.00	45.8 ± 0.2	27.8 ± 2.1	87.0 ± 6.6	0.52 ± 0.08
0.25	0.26	0.28	47.2 ± 0.2	28.9 ± 2.5	90.2 ± 7.8	0.75 ± 0.04
0.50	0.53	0.63	49.3 ± 0.1	29.7 ± 1.9	92.2 ± 5.9	0.83 ± 015
0.75	0.81	1.07	52.1 ± 0.2	31.0 ± 2.5	95.1 ± 7.5	0.22 ± 0.11
1.00	1.11	1.62	54.1 ± 0.1	32.7 ± 1.5	100 ± 4.6	0.46 ± 0.08
1.25	1.43	2.31	55.0 ± 0.2	33.9 ± 3.7	103 ± 11.2	0.78 ± 0.08
1.50	1.76	3.17	57.5 ± 0.3	33.5 ± 3.4	101 ± 10.3	0.64 ± 0.25
1.75	2.12	4.26	59.3 ± 0.1	37.2 ± 2.7	112 ± 8.1	0.78 ± 0.08
2.00	2.50	5.65	61.4 ± 0.1	35.9 ± 2.2	107 ± 6.6	0.60 ± 0.15
2.25	2.90	7.42	63.3 ± 0.2	37.6 ± 3.3	112 ± 9.7	0.73 ± 0.20
2.50	3.32	9.71	65.2 ± 0.1	38.6 ± 2.0	114 ± 5.9	0.45 ± 0.12
2.75	3.78	12.68	66.6 ± 0.2	37.1 ± 2.6	109 ± 7.6	0.66 ± 0.17
3.00	4.27	16.59	67.7 ± 0.1	39.5 ± 2.3	116 ± 6.9	0.70 ± 0.16
3.25	4.79	21.81	68.5 ± 0.2	41.4 ± 4.4	121 ± 13.0	0.90 ± 0.04
3.50	5.35	28.89[a]	69.8 ± 0.3	39.8 ± 6.4	116 ± 19.5	0.93 ± 0.07
3.75	5.96	38.70[a]	71.5 ± 0.2	41.5 ± 3.3	120 ± 9.7	0.83 ± 0.06
4.00	6.61	52.61[a]	73.2 ± 0.2	42.6 ± 5.2	123 ± 15.1	0.21 ± 0.26

[a] Thermodynamic activities of GB were extrapolated from the data of ref *31*.

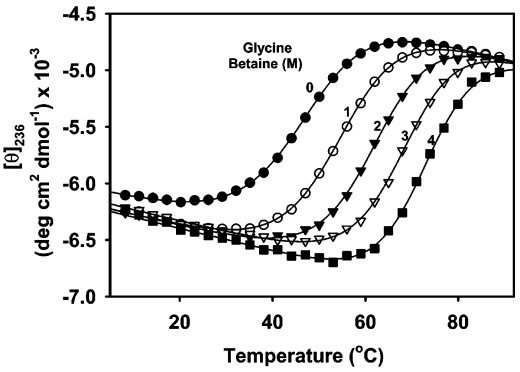

FIGURE 1: Thermal unfolding transitions of lacI HTH at representative GB concentrations (25 mM K_2HPO_4, pH 7.3). Averaged ellipticities $[\theta]_{236}$ for triplicate experiments (standard error ± 3%) are plotted vs temperature; regression fits were obtained using a two-state equilibrium unfolding model (*30*) with a constant $\Delta C^\circ_{p,obs}$ of unfolding. GB concentrations are 0 (●), 1 (○), 2 (▼), 3 (▽), and 4 M (■).

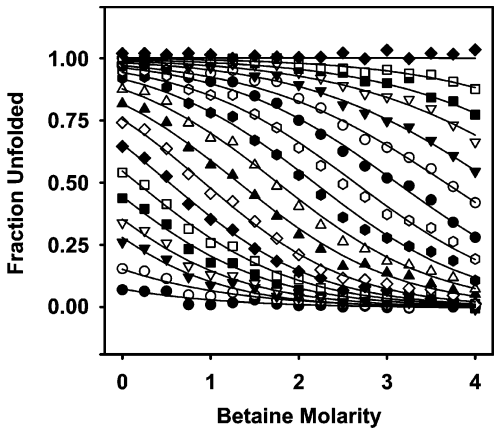

FIGURE 2: Isothermal GB-induced folding transitions of lacI HTH as monitored by circular dichroism at 236 nm and converted to fraction unfolded using linear baselines at the following temperatures (starting at the bottom left of the figure): 23.2 (●), 32.2 (○), 38.1 (▼), 41.1 (▽), 44.1 (■), 47.1 (□), 50.1 (◆), 53.1 (◇), 56.0 (△), 59.0 (▲), 62.0 (⬠), 65.0 (⬢), 68.0 (●), 71.0 (○), 74.0 (▼), 76.9 (▽), 79.9 (■), 82.9 (□), and 94.9 °C (◆). Fits assume a GB-concentration-independent (but not a temperature-independent) *m*-value.

of ΔG°_{obs} of unfolding over a 1 M interval of C_3:

$$m\text{-value} \equiv -\frac{\Delta(\Delta G^\circ_{obs})}{\Delta C_3} \cong -\left(\frac{\partial \Delta G^\circ_{obs}}{\partial C_3}\right)_T \qquad (7)$$

where $\Delta G^\circ_{obs} = -RT \ln K_{obs}$ is the standard observed free energy change for unfolding. Individual transitions (though completely cooperative) extend over a wide range of GB concentration because the change in accessible surface area of the protein upon unfolding is relatively small (*30*).

Deviations of the data of Figure 2 from the fit to the two-state model with a GB concentration-independent *m*-value are small. The GB concentration independence of the *m*-value and consequent extended linear dependence of ΔG°_{obs} on GB molarity, though empirically consistent with the behavior observed in urea (*30*), is unexpected because the magnitude of the thermodynamic nonideality of aqueous GB solutions (*31*) is much larger than that observed for aqueous urea solutions. An explanation of this behavior in the context of the solute partitioning model is provided elsewhere (*32*).

Stabilization of the Folded lacI HTH by GB Is Largely Entropic. The temperature dependences of the GB *m*-value (eq 7) and of the corresponding quantity (dln K_{obs}/dC_3) were determined using the data of Figure 2 to investigate enthalpic and entropic contributions of GB to lacI HTH stability. Values of ΔG°_{obs} and ln K_{obs} were calculated as a function of GB concentration for each isothermal folding curve in Figure 2 and divided into four 1 M concentration intervals from 0 to 4 M. Data in each interval at each temperature were fit to straight lines, the slopes of which are plotted as a function of temperature in Figure 3, panels A and B. This procedure allows an unambiguous separation of variations in the *m*-value (also dln K_{obs}/dC_3) caused by changes in temperature from those caused by changes in GB concentration. Figure 3, panels C and D shows that d*m*-value/dT = 2.5 ± 1.1 cal mol^{-1} M^{-1} K^{-1}, independent of GB concentration up to at least 3 M, and that d(dln K_{obs}/dC_3)/dT = (0 ± 1) × 10^{-3} M^{-1} K^{-1}.

The observation that dln K_{obs}/dC_3 is independent of temperature within uncertainty indicates that ΔH°_{obs} of unfolding does not depend significantly GB concentration, that is, dΔH°_{obs}/dC_3 = 0 ± 200 cal mol^{-1} M^{-1} (at 50 °C). The significant dependence of the GB *m*-value on temper-

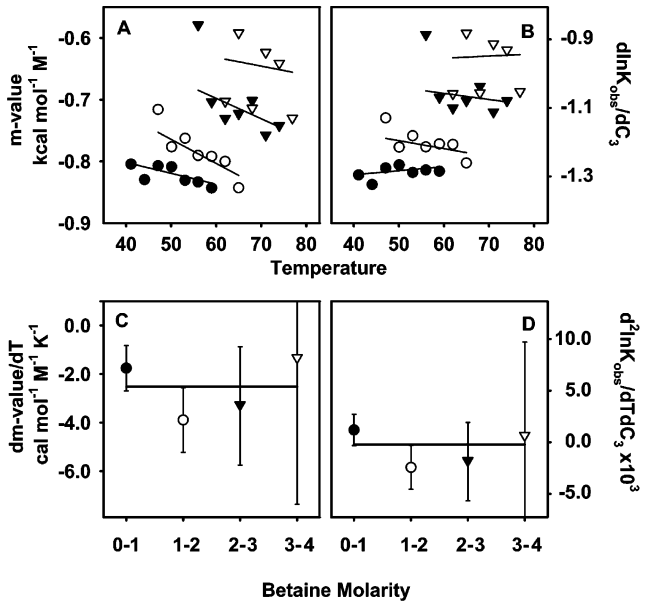

FIGURE 3: The *m*-value (panel A) and dln K_{obs}/dC_3 (panel B) for GB-induced folding of lacI HTH as a function of temperature for different GB concentration ranges. Data points correspond to values of the *m*-value (panel A) and of the closely related quantity dln K_{obs}/dC_3 (panel B) in the concentration ranges 0−1 (●), 1−2 (○), 2−3 (▼), and 3−4 M (▽) GB. The experimental scatter, which increases significantly at higher GB concentrations, is representative of the error associated with individual data points. Values of the slopes of the linear regression fits in panels A and B give the temperature dependence of the *m*-value (panel C) and dln K_{obs}/dC_3 (panel D) at different GB concentration ranges. Horizontal lines in panels C and D are weighted averages of the data in those plots.

ature indicates (*30*) that ΔS°_{obs} of unfolding decreases with increasing GB concentration: $d\Delta S^\circ_{obs}/dC_3 = -2.5 \pm 1.1$ eu M^{-1}. Although our data does not preclude a modest enthalpic contribution to the stabilization (or destabilization) of lacI HTH by increasing GB concentration, the error analysis indicates that any such contribution (±200 cal mol^{-1} M^{-1}) is small relative to the *m*-value and therefore that stabilization arises primarily, if not entirely, from the entropically unfavorable interaction of GB with the lacI surface exposed upon unfolding. For lacI HTH unfolding in urea, $d\Delta S^\circ_{obs}/dC_3 = -0.67 \pm 0.30$ cal mol^{-1} M^{-1}, so the interaction of urea with the surface exposed upon unfolding lacI HTH at 25 °C is also entropically unfavorable. In the case of urea, favorable enthalpic interactions ($d\Delta H^\circ_{obs}/dC_3 = -660 \pm 90$ cal mol^{-1} M^{-1} at 25 °C) overcome this entropic cost, leading to accumulation of urea near the newly exposed protein surface. By contrast, GB appears to have no similar net favorable enthalpic contribution, the unfavorable entropy dominates, and GB is excluded from the surface exposed upon unfolding. If the two-component activity coefficient of GB in water were significantly temperature-dependent, that would also contribute to the temperature dependence of the *m*-value, as observed for urea (*30*).

Quantifying Exclusion of GB from the Surface Exposed upon Unfolding the lacI HTH. At low GB concentrations, the *m*-value is directly related to the difference between preferential interaction coefficients for the unfolded and folded states (*30*, *39*):

$$(C_3 \rightarrow 0): \qquad \frac{m\text{-value}}{RT} = \left(\frac{\partial \ln K_{obs}}{\partial C_3}\right)_T \cong \frac{\Delta\Gamma_{\mu_3}}{m_3} \qquad (8)$$

Equation 8 neglects the concentration-dependent nonideality of GB solutions and differences between concentration scales and is thus only strictly valid in the limit of very low GB concentrations. Analyses of dln K_{obs}/dC_3 for protein unfolding at higher solute concentrations have been developed (*32*, *35*, *39*). With the conventional assumption (*39*) of additivity of contributions to $\Delta\Gamma_{\mu_3}$ from different regions of protein surface, $\Delta\Gamma_{\mu_3}$ is interpreted as the preferential interaction coefficient of GB with that surface which is newly exposed in the unfolding process:

$$\Delta\Gamma_{\mu_3} = \Gamma^\Delta_{\mu_3} \qquad (9)$$

where the superscript Δ denotes the surface exposed in unfolding as distinct from the entire surface of the unfolded state (*4*, *30*, *39*). Extrapolation of the low GB concentration (0−1 M) *m*-value data in Figure 3 to 25 °C, using d*m*-value/d$T = 2.5 \pm 1.1$ cal M^{-1} K^{-1} yields an *m*-value of -783 ± 112 at 25 °C; from eq 8, $\Gamma^\Delta_{\mu_3}/m_3 = -1.32 \pm 0.19$ (Table 3). This value of $\Gamma^\Delta_{\mu_3}/m_3$ indicates that the extent of preferential exclusion of GB from the surface exposed upon unfolding the lacI HTH near room temperature is relatively small, as compared to the value expected for complete exclusion from a monolayer of water at this surface, for which $\Gamma^\Delta_{\mu_3}/m_3$ would equal −6.9 (*5*); $\Gamma^\Delta_{\mu_3}/m_3$ for exclusion of GB is more comparable in magnitude to the extent of accumulation of urea at this surface ($\Gamma^\Delta_{\mu_3}/m_3 = 0.76 \pm 0.02$) (*30*).

Quantifying Exclusion of GB from Folded Protein Surface. To characterize the interactions between GB and folded protein surface, we have performed osmometric measurements on GB solutions containing BSA and lysozyme (HEWL). Osmolality differences, Δ_{23}Osm, for three-component GB−BSA−H_2O solutions (calculated with eq 1) and the analogous quantity $\Delta_{[2,4]3}$Osm for four-component GB−HEWL−salt−H_2O solutions (calculated with eq 5) are plotted vs GB molality (m_3) in Figure 4. Molalities of protein (m_2), and of salt (m_4) where present, were held constant at the indicated values, and m_3 was varied as indicated. In both three- and four-component systems, ΔOsm is the osmolality increment arising from GB−protein interactions, analysis of which yields μ_{23} (eq 2) and ultimately Γ_{μ_3} (eq 3). At each molality of BSA or HEWL, ΔOsm is observed to increase strongly with increasing GB molality. At each GB molality, ΔOsm also increases strongly with increasing molality of either BSA or HEWL. With HEWL, the different molalities of supporting electrolyte had no significant effect on ΔOsm (Figure 4).

The positive differences between the osmolalities of GB solutions containing the folded proteins BSA or HEWL and the sum of osmolalities of the corresponding two-component solutions (i.e., ΔOsm; eqs 1, 5) indicate unfavorable interactions between GB and each of these folded proteins relative to interactions with water, which result in local exclusion of GB from the vicinity of the protein surface (preferential hydration). Derivatives of the biopolymer chemical potential with respect to GB concentration (μ_{23} or $\mu_{[2,4]3}$, eq 2) are reported in Table 3. The extent of exclusion of GB from these folded protein surfaces is quantified by the dependences

Table 3: Preferential Interaction Coefficients and Related Parameters for the Interaction of Glycine Betaine with Folded Biopolymers and for the Effect of Glycine Betaine on Protein Unfolding

biopolymer surface	μ_{23}[a] (kcal mol^{-1} m^{-1})	$\Gamma_{\mu_3}/m_3^{bulk}$ (m^{-1})	$10^3\Gamma_{\mu_3}/(m_3^{bulk}$ASA) ($m^{-1}$ Å^{-2})
lacI HTH unfolding (ASA$^{\Delta}$)		-1.32 ± 0.19[e]	-0.38 ± 0.05
folded HEWL[b]	2.8 ± 1.3	-3.1 ± 1.1[c]	-0.47 ± 0.17
folded BSA[b]	21.7 ± 3.4	-23.1 ± 1.4[c]	-0.83 ± 0.05
duplex monosomal calf thymus DNA[b]	0.22 ± 0.008[d]	-0.30 ± 0.02[d]	-1.8 ± 0.1
Proposed Interpretation from Two-Parameter Fit			
100% anionic oxygen surface			-4.0 ± 0.3
100% polar amide surface			-1.1 ± 0.1

[a] Evaluated from VPO ΔOsm using eq 2. [b] VPO data were obtained primarily at 25 °C; however, no difference was observed between VPO data at 25 and 37 °C. [c] Evaluated from eq 3 using μ_{23} and μ_{33} (eq 4). [d] Per nucleotide; from Hong et al. (*65*). [e] Calculated at 25 °C from extrapolated GB *m*-value (see Results).

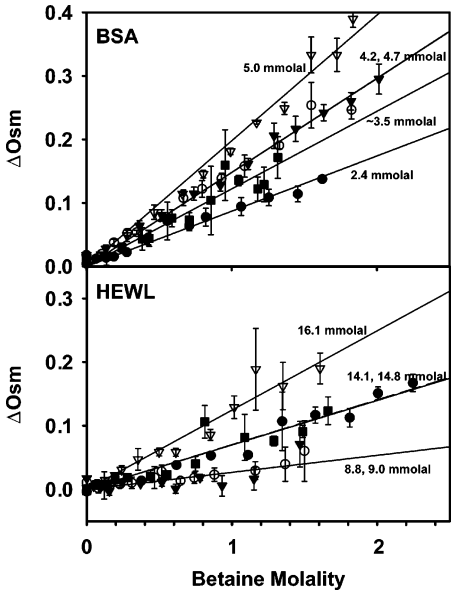

FIGURE 4: ΔOsm representation of VPO results for interactions of glycine betaine with folded bovine serum albumin (BSA, top) and hen egg white lysozyme (HEWL, bottom). The top panel plots osmolality differences, ΔOsm (eq 1), as a function of GB molality for experiments at BSA concentrations of 2.4 (●), 3.3−3.9 (■), 4.2 (○), 4.7 (▼), and 5.0 m*m* (▽). The bottom panel plots ΔOsm (eq 5) as a function of GB molality for the following HEWL, buffer, and salt concentrations: 8.8 m*m* HEWL, 4.4 m*m* HEPES, 8.9 m*m* NaCl (▼); 9.0 m*m* HEWL, 4.4 m*m* HEPES, 8.8 m*m* NaCl (○); 14.1 m*m* HEWL, 126 m*m* KCl (■); 14.8 m*m* HEWL, 7.3 m*m* HEPES, 14.5 m*m* NaCl (●); 16.1 m*m* HEWL, 7.9 m*m* HEPES, 15.8 m*m* NaCl (▽).

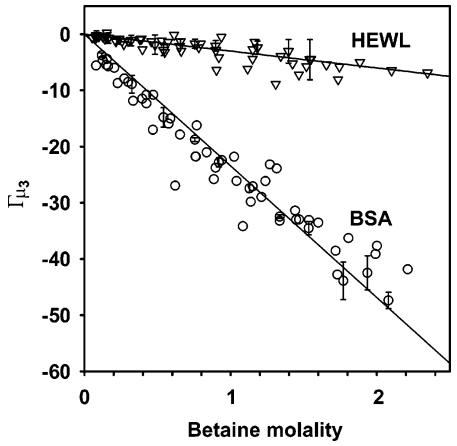

FIGURE 5: Dependences on bulk GB molality of the preferential interaction coefficients Γ_{μ_3} for the interaction of GB with lysozyme (HEWL; ▽) and BSA (○). Estimated uncertainties (±1 SD) for representative HEWL and BSA data sets are shown.

of Γ_{μ_3} on GB molality plotted in Figure 5. For both folded proteins, Γ_{μ_3} is found to be proportional to GB molality, becoming more negative with increasing GB molality. Linear regression, with the requirement of a zero intercept (*41*), gives proportionality constants (see eq 6) $\Gamma_{\mu_3}/m_3^{bulk} = -23.1 \pm 1.4$ (1 SD) for BSA and -3.1 ± 1.1 for HEWL (Table 3). The present all-gravimetric VPO result for GB and BSA revises our previously reported value (*5*, *33*), obtained using a volumetric transfer of BSA, which we have since found caused a systematic overestimate of Γ_{μ_3} (see Experimental Procedures). Within experimental uncertainty, values of $\Gamma_{\mu_3}/m_3^{bulk}$ are independent of protein molality and, in the case of HEWL, are also independent of the molality of the supporting 1:1 electrolyte. Values of the derivative $d\Gamma_{\mu_3}/dm_3$ estimated from data of Arakawa and Timasheff (*22*) ($d\Gamma_{\mu_3}/dm_3 = -26.1 \pm 7.0$ for BSA and $d\Gamma_{\mu_3}/dm_3 = -4.0 \pm 1.4$ for HEWL) are in good agreement with our reported values of $\Gamma_{\mu_3}/m_3^{bulk}$. However, while values of Γ_{μ_3} determined from these densimetric measurements on dialyzed solutions (*22*) are well approximated as a linear function of m_3, the zero-concentration intercepts differ significantly from zero, the intercept expected from both the solute partitioning model (*5*) and a fundamental thermodynamic analysis for nonelectrolytes (*42*).

DISCUSSION

Normalization by ASA to Compare Preferential Interactions of GB with Different Biopolymer Surfaces. Preferential interactions of GB with the different biopolymer surfaces investigated in this study are characterized by the proportionality constants $\Gamma_{\mu_3}/m_3^{bulk}$ listed in Table 3. In all cases, $\Gamma_{\mu_3}/m_3^{bulk}$ is negative, indicating exclusion of GB from each of these biopolymer surfaces. To permit comparisons of values of $\Gamma_{\mu_3}/m_3^{bulk}$ for the interactions of a solute with different biopolymer surfaces, we proposed that $\Gamma_{\mu_3}/m_3^{bulk}$ be normalized by the total biopolymer ASA to obtain a quantitative measure of the average preferential interaction of GB with a unit area (1 Å^2) of biopolymer surface (*5*, *35*, *39*). In the context of the local−bulk solute partitioning model, division of $\Gamma_{\mu_3}/m_3^{bulk}$ by ASA yields a quantity that (at low m_3^{bulk}) is dependent only on the average partition coefficient of the solute and the average hydration of the biopolymer surface (see eq 6).

Comparison of values of $\Gamma_{\mu_3}/(m_3^{bulk}ASA)$ for different biopolymer surfaces indicates whether the average preferential interaction of GB per Å^2 of these biopolymer surfaces is a function of surface composition. For example, from the observation (*44*) that urea and GuHCl *m*-values for unfolding globular proteins are proportional to the ASA exposed upon unfolding (designated ASA$^\Delta$), we concluded that the preferential interactions ($\Gamma_{\mu_3}/m_3^{bulk}$) of urea and GuHCl with these surfaces are proportional to ASA$^\Delta$ at fixed small solute concentration, so that the quantity $\Gamma^\Delta_{\mu_3}/(m_3\ ASA^\Delta)$ is the same for unfolding of all globular proteins investigated. From *m*-values for the destabilizing effects of these denaturants on alanine-based α-helices (*45*, *46*), we concluded that values of $\Gamma^\Delta_{\mu_3}/(m_3ASA^\Delta)$ for α-helices are approximately four times larger than the corresponding values for unfolding of globular proteins (*39*). This 4-fold difference in $\Gamma^\Delta_{\mu_3}/(m_3ASA^\Delta)$ correlates with a 3- to 4-fold larger fraction of polar peptide (amide) surface in the ASA$^\Delta$ of α-helix melting and led to the proposal that these denaturants preferentially accumulate only at polar peptide (amide) surface (*39*). This proposal has been recently tested for the interactions of urea with nucleic acid surfaces (*65*).

Values of $\Gamma^\Delta_{\mu_3}/m_3^{bulk}$ together with the corresponding reduced quantity $\Gamma_{\mu_3}/(m_3^{bulk}ASA)$ for interactions of GB with the biopolymer surfaces investigated here are tabulated in Table 3. For the surfaces exposed in unfolding, ASA$^\Delta$ was calculated using a fully extended chain model of the unfolded state (*32*). This model has been successfully applied to analyze both heat capacity changes (*44*, *47*, *48*) and *m*-values for protein unfolding (*39*, *44*); use of a less solvent-accessible model of the unfolded state (e.g., ref *49*) would reduce ASA$^\Delta$ and therefore increase the magnitude of $\Gamma^\Delta_{\mu_3}/(m_3ASA^\Delta)$ for the surface exposed in unfolding the lacI HTH.

Table 3 indicates that the reduced quantity $\Gamma_{\mu_3}/(m_3^{bulk}ASA)$ is negative, and that its magnitude increases from approximately $0.4 \times 10^{-3}\ m^{-1}$ Å^{-2} for the interaction of GB with the surface exposed in unfolding the lacI HTH to $0.5 \times 10^{-3}\ m^{-1}$ Å^{-2} for folded HEWL surface, $0.8 \times 10^{-3}\ m^{-1}$ Å^{-2} for folded BSA surface, and $1.8 \times 10^{-3}\ m^{-1}$ Å^{-2} for native DNA surface. From the large differences in the magnitude of $\Gamma_{\mu_3}/(m_3^{bulk}ASA)$ for native DNA surface, folded protein surfaces, and the surface exposed in unfolding the lacI HTH, we conclude that these biopolymer surfaces do not form a homologous series with regard to their interactions with GB and, therefore, that differences in surface composition give rise to differences in preferential interactions. The correlation of these reduced preferential interaction coefficients with surface composition is discussed in the following section.

Extent of Exclusion of GB Correlates with the Fraction of Anionic Oxygen Surface of Biopolymers. Compositions of the various biopolymer surfaces for which we have determined preferential interaction coefficients of GB are summarized in Table 1. Qualitatively, we observe that values of $\Gamma_{\mu_3}/(m_3^{bulk}ASA)$ for the interactions of GB with these surfaces (Table 3) correlate most strongly with the fraction of anionic biopolymer surface (i.e., anionic oxygens of protein carboxylates and DNA phosphates) from Table 1. Anionic phosphate oxygens constitute 44% of the ASA of native DNA, but anionic carboxylate oxygens constitute only 2% of the surface exposed in unfolding the lacI HTH; carboxylate oxygens are 16% of the ASA of folded BSA, but only 4% of the ASA of folded HEWL. Figure 6, which plots the normalized extent of exclusion of GB (i.e., $\Gamma_{\mu_3}/(m_3^{bulk}ASA)$) as a function of the fraction of biopolymer anionic ASA, shows the strong increase in the extent of exclusion of GB per Å^2 of total biopolymer surface as the anionic contribution to the surface composition increases. If GB were preferentially excluded only from anionic surface, then $\Gamma_{\mu_3}/(m_3^{bulk}ASA)$ would be directly proportional to the fraction of anionic surface; the data in Figure 6 would fit a line through the origin like that drawn through the point for duplex DNA. Instead, systematic deviations from such a proportionality of $\Gamma_{\mu_3}/(m_3^{bulk}ASA)$ to the fraction of anionic surface are observed, which indicate an additional contribution to exclusion of GB that increases in significance as the fraction of anionic surface decreases. From amino acid transfer data, Bolen and co-workers have proposed that exclusion of osmolytes, including GB, from the peptide backbone is the basis of the protein-stabilizing effect of these osmolytes (*25*, *26*, *50*−*52*). The ASA of duplex DNA is 44% anionic oxygen surface and only 2.5% polar amide surface (see Table 1 and definitions in Experimental Procedures), so the reference line in Figure 6 serves as a starting point for a visual analysis of the contribution of amide surface to exclusion of GB from the protein surfaces investigated. Folded lysozyme surface and the surface exposed upon unfolding lacI HTH exhibit the largest deviations from the reference line, while folded BSA surface exhibits a much smaller deviation. For the two folded proteins, the magnitudes of these deviations are consistent with the 2-fold greater contribution of polar amide surface to ASA of lysozyme (27.3%) as compared to BSA (14.6%).

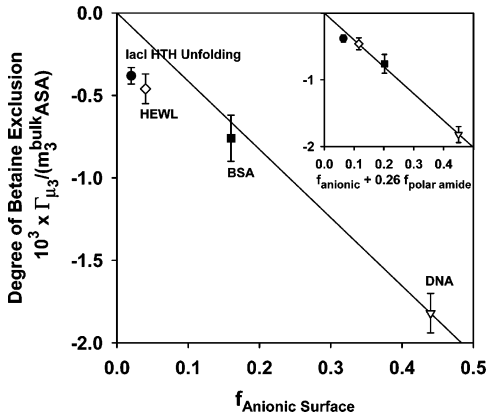

FIGURE 6: The correlation between the extent of GB exclusion per Å^2 of biopolymer surface, quantified by $\Gamma_{\mu_3}/(m_3^{bulk}ASA)$ (see eqs 3 and 9), and the fraction of anionic biopolymer surface (data of Table 3). Inset replots $\Gamma_{\mu_3}/(m_3^{bulk}ASA)$ vs a composite surface composition variable, in which the fraction of polar amide surface is weighted by the numerical factor 0.26 (see text). The line shows the expected proportionality between $\Gamma_{\mu_3}/(m_3^{bulk}ASA)$ and the composite composition variable, based on the GB exclusion parameters for anionic and polar amide surface.

A two-parameter fit to the data of Table 3 for the three folded biopolymer surfaces investigated yields intrinsic values of $\Gamma_{\mu_3}/(m_3^{bulk}ASA)$ for 100% anionic oxygen surface ($(-4.0 \pm 0.3) \times 10^{-3}\ m^{-1}$ Å^{-2}) and 100% polar amide surface ($(-1.1 \pm 0.3) \times 10^{-3}\ m^{-1}$ Å^{-2}). According to this analysis, more than 99% of the observed exclusion of GB from duplex DNA surface arises from its exclusion from

anionic oxygen surface. For folded BSA, approximately 80% of the observed exclusion is from anionic (carboxylate) oxygen surface and 20% from polar amide surface. For folded lysozyme, GB exclusion is primarily from polar amide surface (60%) and secondarily (40%) from anionic oxygen. For the surface exposed upon unfolding lacI HTH, use of the above intrinsic parameters for anionic oxygen and polar amide surface provides near-quantitative agreement with the experimental result: the predicted value of $\Gamma_{\mu_3}/(m_3^{\text{bulk}}\text{ASA})$ is $(-0.27 \pm 0.05) \times 10^{-3}\ m^{-1}\ \text{Å}^{-2}$, as compared with the observed value of $(-0.38 \pm 0.05) \times 10^{-3}\ m^{-1}\ \text{Å}^{-2}$. To the extent that this difference is significant, it may result either from an overestimate of ASA^{Δ} or from an additional, smaller-magnitude contribution of nonpolar surface (which makes up 73% of ASA^{Δ} for lacI HTH) to exclusion of GB. (A four-parameter fit including cationic and nonpolar surface along with anionic and amide surface gives values for $\Gamma_{\mu_3}/(m_3^{\text{bulk}}\text{ASA})$ of $-3.9 \times 10^{-3}\ m^{-1}\ \text{Å}^{-2}$ for anionic surface, $-0.8 \times 10^{-3}\ m^{-1}\ \text{Å}^{-2}$ for amide surface, $-0.3 \times 10^{-3}\ m^{-1}\ \text{Å}^{-2}$ for nonpolar surface, and $0.4 \times 10^{-3}\ m^{-1}\ \text{Å}^{-2}$ for cationic surface. Values for anionic and polar amide surface are consistent with the two-parameter analysis; the values for nonpolar and cationic surface are not significantly different from zero, given the uncertainties ($\pm 0.3 \times 10^{-3}$) determined in the two-parameter fit.)

From the above two-parameter fit, exclusion of GB from the polar amide surface exposed upon unfolding the lacI HTH is predicted to contribute approximately two-thirds of the calculated total stabilizing effect of GB in this system, consistent with Bolen's osmophobic hypothesis of protein stabilization (*25*). The exclusion of GB from anionic oxygen surface of biopolymers, which is four times as large in magnitude (per Å^2) as its exclusion from polar amide surface, is almost certainly the dominant contributor to its osmoprotectant effect in vivo, as discussed below. The inset to Figure 6 replots the GB exclusion data for the four biopolymer surfaces investigated as a function of a composite surface composition variable, defined as the sum of the fraction of anionic surface and 26% of the fraction of polar amide surface. The weighting factor 26% is the ratio of intrinsic values of $\Gamma_{\mu_3}/(m_3^{\text{bulk}}\text{ASA})$ for polar amide and anionic surface $(0.26 = (1.1 \times 10^{-3})/(4.0 \times 10^{-3}))$. Clearly GB exclusion data for the folded protein and duplex DNA surfaces are proportional to this composite composition variable, and the point for lacI HTH ASA^{Δ} deviates only slightly from the line.

From the intrinsic values of $\Gamma_{\mu_3}/(m_3^{\text{bulk}}\text{ASA})$ for anionic oxygen and polar amide surface calculated above, lower bound values on the hydration of these surfaces (b_1°) are obtained from the local−bulk solute partitioning model (eq 6). For anionic oxygen surface, the product $(K_P^{\circ} - 1)b_1^{\circ} = -0.22 \pm 0.02\ \text{H}_2\text{O}\ \text{Å}^{-2}$. If GB is completely excluded ($K_P^{\circ} = 0$, i.e., zero local concentration) from anionic oxygen surface of proteins, then $b_1^{\circ} = 0.22 \pm 0.02\ \text{H}_2\text{O}\ \text{Å}^{-2}$. (If GB is incompletely excluded from this surface ($1 > K_P^{\circ} > 0$), then $b_1^{\circ} > 0.22\ \text{H}_2\text{O}\ \text{Å}^{-2}$.)

Since a monolayer of water of hydration is approximately $0.11\ \text{H}_2\text{O}\ \text{Å}^{-2}$(*5*), the hydration of anionic carboxylate oxygen surface is at least two layers of water or at least 15−18 H_2O molecules per average carboxylate residue (∼65−80 Å^2 of anionic oxygen surface as calculated for lacI HTH surfaces). If polar amide surface is the only other type of surface contributing to exclusion of GB for the systems investigated, then an analogous calculation for this type of surface yields $(K_P^{\circ} - 1)b_1^{\circ} = -0.06 \pm 0.02\ \text{H}_2\text{O}\ \text{Å}^{-2}$. Since the hydration of polar amide surface probably is at least a monolayer, it is therefore likely that GB is not completely excluded from polar amide surface ($1 > K_P^{\circ} > 0$). Further studies with other biopolymer surfaces and other osmolytes are in progress to extend and refine this analysis.

Burling et al. (*53*) determined water density as a function of radial distance from crystalline protein surface. They found the density maximum was closer to oxygen surface (∼3.0 Å) than to nitrogen surface (∼3.2 Å) or carbon surface (∼3.8 Å). No distinction was made between charged and uncharged nitrogen and oxygen surfaces. However, the data suggest stronger hydration of oxygen surface than other surfaces. From crystallographic data and measurements of dehydration of protein films observed by FTIR, Poole and Barlow (*54*) calculated greater dehydration enthalpies for waters associated with carboxylate groups than with amide carbonyl oxygens. Molecular dynamics simulations by Pettitt and coworkers (*55*) agree with the data of Burling et al. (*53*) and indicate that water density is affected only by the nature of the closest protein atom. Combined, the above observations imply stronger hydration of anionic oxygen surface than of other surfaces on proteins, including amide oxygen surface. Our results are consistent with this conclusion. Experimental data indicating strong hydration of anionic phosphate oxygens on DNA (*56*, *57*) are discussed elsewhere (*65*).

Model Compound Data Indicate that Hydration of Carboxylate Oxygens and the Inability To Form Intermolecular (GB−GB) Hydrogen Bonds Dominate GB Nonideality in Two-Component Solutions. Molal-scale activity coefficient data for two-component aqueous solutions of GB, glycine, and tetramethylammonium and acetate salts provide insights into the molecular basis of exclusion of GB from anionic carboxylate oxygens on biopolymers. These activity coefficients are referenced to an ideal dilute-solution (i.e., hydrated solute) standard state. Neglecting a typically small contribution due to ideal mixing entropy, molal-scale activity coefficients of less than unity indicate relatively favorable solute−solute interactions and the tendency of the solute to accumulate near or associate with itself; activity coefficients greater than unity indicate that solute−water interactions are more favorable (or less unfavorable) than solute−solute interactions.

Glycine betaine and its close relative glycine exhibit very different dependences of activity coefficient on concentration in water, indicating very different balances between self-interactions and interactions with water for these two solutes (Figure 7). Glycine, like urea, exhibits relatively small deviations from ideal dilute solution behavior over the range of interest (*58*). Attractive glycine−glycine interactions must therefore be sufficiently favorable to compensate for excluded volume effects and hydration effects as glycine concentration increases, resulting in an activity coefficient for glycine that is slightly less than unity even at 3 *m* glycine. However, complete methylation of the amino group of glycine to form GB eliminates the capacity of GB to hydrogen bond with itself. The thermodynamic manifestation of these changes in the cationic moiety is a large increase in activity coefficient with increasing solute molality (Figure 7). Rather than

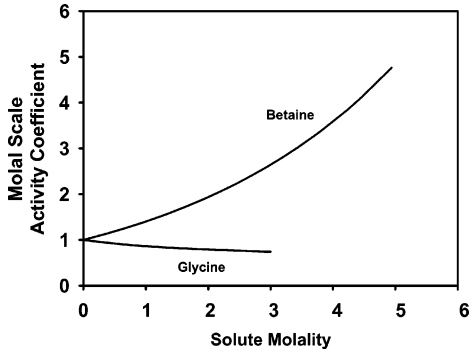

FIGURE 7: Molal scale two-component activity coefficients for aqueous solutions of GB (*31*) and of glycine (*58*) as a function of solute molality.

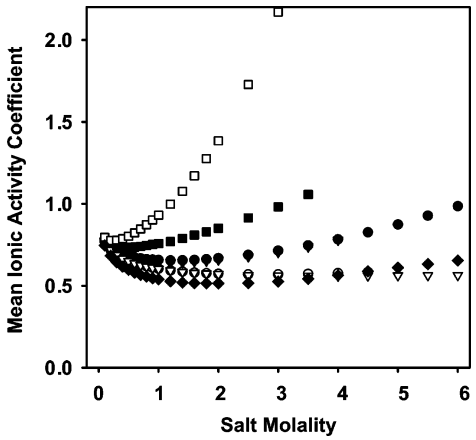

FIGURE 8: Molal scale mean ionic activity coefficients, $\gamma_{\pm}^{m}$, for univalent salts in aqueous solution as a function of salt molality. Different symbols correspond to NaCl (●), KCl (○), KF (▼), NH_4-Cl (▽), NaAcetate (■), TMAF (□), and TMACl (◆).

exhibiting the slightly favorable net self-interaction of glycine, GB remains strongly hydrated (i.e., interacts preferentially with water instead of other GB) in aqueous solution at all concentrations.

An estimate of the hydration of GB is readily obtained from literature data (*31*) for the concentration dependence of its osmotic coefficient φ, defined as the ratio of the solution osmolality (Osm) to the molal GB concentration (m_{GB}). If the only contribution to osmotic nonideality is from the reduction in the amount of free water as a consequence of binding h molecules of water of hydration to each molecule of GB (*36*), then

$$\varphi \equiv \frac{\mathrm{Osm}}{m_{GB}} = 1 + 0.018 m_{GB}\left(h + \frac{1}{2}\right) + (0.018 m_{GB})^2\left(h^2 - h + \frac{1}{3}\right) + \ldots \quad (10)$$

where m_{GB} is calculated per kilogram of total water. Equation 10 provides a good fit at low to moderate GB concentrations (<1 *m*) but at higher GB molality exhibits curvature opposite to that of the experimental data in Figure 7. An improved fit is obtained by replacing the constant hydration number, h, with a solute-concentration-dependent term, $h = h_0 + m_{GB}h_1$. With $h_0 = 8.5$ and $h_1 = -0.5$, eq 10 gives a much better fit, with the correct curvature, to GB osmotic coefficient data up to 4.9 *m* than that obtained using a constant hydration number (fits not shown). This analysis may provide a minimum estimate of the hydration of GB: ~8.5 osmotically inactive water molecules around each GB molecule at low m_{GB}, decreasing to ~6 at 4.9 *m*. A molecular dynamics simulation of GB in aqueous solution (*59*) predicts more water of hydration than h_0 but also predicts a similar relative reduction in the number of waters within 3.5 Å of each GB molecule as GB concentration increases from 0 to 3.3 *m*. These considerations and the position of carboxylate anions (acetate, glutamate) in the Hofmeister series (*60*) both suggest that the thermodynamic nonideality of GB is dominated by the strong hydration of the carboxylate anion. Additional insight into the physical origin of the distinctive characteristics of the activity coefficient of GB as a function of its concentration is obtained by comparing it with activity coefficients of some simple electrolytes.

Molal scale mean ionic activity coefficients of acetate and fluoride salts of alkali metals and ammonium (*61*), reproduced in Figure 8, exhibit concentration dependences similar to most other 1:1 salts; tetramethylammonium (TMA) chloride and bromide behave analogously (*62*, *63*). For these salts, the activity coefficient decreases up to ~1 *m* and then gradually increases toward unity at higher salt concentration. Mean ionic activity coefficients of TMA fluoride and, to a lesser extent, sodium acetate deviate from this pattern. For TMAF, a minimum is observed near 0.2 *m*. Above 0.2 *m*, the activity coefficient of TMAF increases strongly with increasing m_3 and exceeds unity above 1 *m*. Extensive hydration of F^- and the lack of hydrogen bonding and of strong electrostatic interactions between the hydrated F^- anion and the low charge density TMA cation must be responsible for the large positive deviation from ideal behavior of TMAF. Analogously, the lack of favorable interactions between the quaternary ammonium group and carboxylates of GB must give rise to its strong nonideality at high concentration. Similar considerations explain the exclusion of GB from anionic protein residues. Since cationic protein moieties more closely resemble the monosubstituted ammonium of glycine than the quaternary ammonium of GB, the present data and discussion are consistent with our finding that GB is excluded more strongly from anionic protein residues than from cationic ones.

How GB Functions as an Effective Osmoprotectant and a Compatible Solute in the E. coli Cytoplasm. The effectiveness of a solute as an osmoprotectant is judged by its ability to increase cytoplasmic osmolality when its cytoplasmic concentration is increased by transport or biosynthesis. Per mole of solute particles, glycine betaine is much more effective than other *E. coli* osmolytes (e.g., proline, trehalose, potassium glutamate) in increasing cytoplasmic osmolality (*6*). This effect is not primarily a consequence of the fact that the osmotic coefficient of 1 *m* GB is ~10% higher than that of 1 *m* trehalose and ~30% higher than that of 0.5 *m* potassium glutamate (KGlu). These differences in osmotic coefficients by themselves account for no more than 25% of the observed effect of replacement of cytoplasmic trehalose, K^+, and Glu^- by a similar molar amount of GB on the amount of cytoplasmic water (*6*). Furthermore, contributions to the osmotic coefficient of the cytoplasm estimated from exclusion of GB and other osmolytes from folded protein surfaces could not explain the observed cytoplasmic osmolality, expecially at high osmolality. Strong preferential exclusion of GB from the anionic surface of cytoplasmic

nucleic acids (especially ribosomal RNA) may explain why the cytoplasmic concentration of GB in free cytoplasmic water (the water not bound to biopolymers as hydration) is so much higher than the corresponding concentrations achieved with other osmolytes, which makes GB the most effective *E. coli* osmoprotectant.

The surface exposed in unfolding a protein (ASA^{Δ}) typically is only minimally anionic (approximately 2% ± 2%) and consists of only approximately 18% ± 2% polar amide surface. Hence changes in GB concentration affect protein stability to a much smaller extent than they would if the composition of the surface exposed in unfolding were as anionic as that of folded BSA or nucleic acids. From the analysis above, we predict that GB will exert the largest effect on protein or nucleic acid processes in which the hydration of large numbers of anionic carboxylate or phosphate groups changes significantly, as in the formation or disruption of multiple surface salt bridges (*64*). Other processes, including protein folding or unfolding, in which the hydration of anionic surface is relatively unaffected are expected to exhibit modest effects of GB concentration, which are also quantitatively predictable from knowledge of the ASA and composition of the biopolymer surface buried or exposed in the process.

Thus we conclude that GB can be both a very effective osmoprotectant and a compatible, only moderately perturbing solute for in vivo biopolymer processes because of the very significant differences in composition between folded biopolymer surface and the surfaces typically involved in folding or other biopolymer processes.

ACKNOWLEDGMENT

CD data were obtained at the University of Wisconsin-Madison Biophysics Instrumentation Facility, which is supported by the University of Wisconsin-Madison and Grants BIR-9512577 (NSF) and S10 RR13790 (NIH).

REFERENCES

1. Yancey, P. H., Clark, M. E., Hand, S. C., Bowlus, R. D., and Somero, G. N. (1982) Living with Water-Stress − Evolution of Osmolyte Systems, *Science 217*, 1214−1222.
2. Record, M. T., Courtenay, E. S., Cayley, D. S., and Guttman, H. J. (1998) Responses of E-coli to osmotic stress: Large changes in amounts of cytoplasmic solutes and water, *Trends Biochem. Sci. 23*, 143−148.
3. Wood, J. M., Bremer, E., Csonka, L. N., Kraemer, R., Poolman, B., van der Heide, T., and Smith, L. T. (2001) Osmosensing and osmoregulatory compatible solute accumulation by bacteria, *Comp. Biochem. Physiol., Part A: Mol. Integr. Physiol. 130*, 437−460.
4. Timasheff, S. N. (1998) Control of protein stability and reactions by weakly interacting cosolvents: The simplicity of the complicated, *Adv. Protein Chem. 51*, 355−432.
5. Courtenay, E. S., Capp, M. W., Anderson, C. F., and Record, M. T. (2000) Vapor pressure osmometry studies of osmolyte-protein interactions: Implications for the action of osmoprotectants in vivo and for the interpretation of "osmotic stress" experiments in vitro, *Biochemistry 39*, 4455−4471.
6. Cayley, S., and Record, M. T. (2003) Roles of cytoplasmic osmolytes, water, and crowding in the response of *Escherichia coli* to osmotic stress: Biophysical basis of osmoprotection by glycine betaine, *Biochemistry 42*, 12596−12609.
7. Low, P. S. (1985) in *Transport processes, iono- and osmoregulation: current comparative approaches* (Gilles, R., and Gilles-Baillien, M., Eds.), Springer-Verlag, New York.
8. Burg, M. B., and Peters, E. M. (1997) Urea and methylamines have similar effects on aldose reductase activity, *Am. J. Physiol.*−*Renal Physiol. 42*, F1048−F1053.
9. Burg, M. B., Peters, E. M., Bohren, K. M., and Gabbay, K. H. (1999) Factors affecting counteraction by methylamines of urea effects on aldose reductase, *Proc. Natl. Acad. Sci. U.S.A. 96*, 6517−6522.
10. Neuhofer, W., Fraek, M. L., and Beck, F. X. (2002) Heat shock protein 72, a chaperone abundant in renal papilla, counteracts urea-mediated inhibition of enzymes, *Pfluegers Arch. 445*, 67−73.
11. Bowlus, R. D., and Somero, G. N. (1979) Solute compatibility with enzyme function and structure: rationales for the selection of osmotic agents and end-products of anaerobic metabolism in marine invertebrates, *J. Exp. Zool. 208*, 137−151.
12. Santoro, M. M., Liu, Y. F., Khan, S. M. A., Hou, L. X., and Bolen, D. W. (1992) Increased Thermal-Stability of Proteins in the Presence of Naturally-Occurring Osmolytes, *Biochemistry 31*, 5278−5283.
13. Fried, M. G., Stickle, D. F., Smirnakis, K. V., Adams, C., MacDonald, D., and Lu, P. (2002) Role of hydration in the binding of lac repressor to DNA, *J. Biol. Chem. 277*, 50676−50682.
14. Anjum, F., Rishi, V., and Ahmad, F. (2000) Compatibility of osmolytes with Gibbs energy of stabilization of proteins, *Biochim. Biophys. Acta 1476*, 75−84.
15. Yancey, P. H., and Somero, G. N. (1979) Counteraction of urea destabilization of protein structure by methylamine osmoregulatory compounds of elasmobranch fishes, *Biochem. J. 183*, 317−323.
16. Yancey, P. H. (2001) Water stress, osmolytes and proteins, *Am. Zool. 41*, 699−709.
17. Bedford, J. J., Schofield, J., Yancey, P. H., and Leader, J. P. (2002) The effects of hypoosmotic infusion on the composition of renal tissue of the Australian brush-tailed possum *Trichosurus vulpecula*, *Comp. Biochem. Physiol., Part B: Biochem. Mol. Biol. 132*, 645−652.
18. Yin, M., Palmer, H. R., Fyfe-Johnson, A. L., Bedford, J. J., Smith, R. A. J., and Yancey, P. H. (2000) Hypotaurine, *N*-methyltaurine, taurine, and glycine betaine as dominant osmolytes of vestimentiferan tubeworms from hydrothermal vents and cold seeps, *Physiol. Biochem. Zool. 73*, 629−637.
19. Bedford, J. J., Harper, J. L., Leader, J. P., Yancey, P. H., and Smith, R. A. J. (1998) Betaine is the principal counteracting osmolyte in tissues of the elephant fish, *Callorhincus millii* (Elasmobranchii, Holocephali), *Comp. Biochem. Physiol., Part B: Biochem. Mol. Biol. 119*, 521−526.
20. Edmands, S. D., Hughs, K. S., Lee, S. Y., Meyer, S. D., Saari, E., and Yancey, P. H. (1995) Time-Dependent Aspects of Osmolyte Changes in Rat-Kidney, Urine, Blood and Lens with Sorbinil and Galactose Feeding, *Kidney Int. 48*, 344−353.
21. Lewis, B. A., Cayley, S., Padmanabhan, S., Kolb, V. M., Brushaber, V., Anderson, C. F., and Record, M. T. (1990) Natural Abundance N-14 and C-13 NMR of Glycine Betaine and Trehalose as Probes of the Cytoplasm of Escherichia-Coli-K12, *J. Magn. Reson. 90*, 612−617.
22. Arakawa, T., and Timasheff, S. N. (1983) Preferential Interactions of Proteins with Solvent Components in Aqueous Amino-Acid Solutions, *Arch. Biochem. Biophys. 224*, 169−177.
23. Auton, M., Baskakov, I., Bolen, C. L., and Bolen, D. W. (2001) On identifying the fundamental forces of osmolyte-induced protein stability, *Biophys. J. 80*, 558a−558a.
24. Bolen, D. W. (1998) Putting backbone into discussions of protein stabilization. *Biophys. J. 74*, A219−A219.
25. Bolen, D. W., and Baskakov, I. V. (2001) The osmophobic effect: Natural selection of a thermodynamic force in protein folding, *J. Mol. Biol. 310*, 955−963.
26. Liu, Y. F., and Bolen, D. W. (1995) The Peptide Backbone Plays a Dominant Role in Protein Stabilization by Naturally-Occurring Osmolytes, *Biochemistry 34*, 12884−12891.
27. Record, M. T., and Anderson, C. F. (1995) Interpretation of Preferential Interaction Coefficients of Nonelectrolytes and of Electrolyte Ions in Terms of a Two-Domain Model, *Biophys. J. 68*, 786−794.
28. Record, M. T., Zhang, W. T., and Anderson, C. F. (1998) Analysis of effects of salts and uncharged solutes on protein and nucleic acid equilibria and processes: A practical guide to recognizing and interpreting polyelectrolyte effects, Hofmeister effects, and osmotic effects of salts, *Adv. Protein Chem. 51*, 281−353.
29. Slijper, M., Boelens, R., Davis, A. L., Konings, R. N., van der Marel, G. A., van Boom, J. H., and Kaptein, R. (1997) Backbone and side chain dynamics of lac repressor headpiece (1−56) and its complex with DNA, *Biochemistry 36*, 249−254.
30. Felitsky, D. J., and Record, M. T. (2003) Thermal and urea-induced unfolding of the marginally stable lac repressor DNA-binding

domain: A model system for analysis of solute effects on protein processes, *Biochemistry 42*, 2202−2217.
31. Smith, P. K., and Smith, E. R. B. (1940) Thermodynamic properties of solutions of animo acids and related substances. V. The activities of some hydroxy- and *N*-methylanimo acids and proline in aqueous solution at twenty-five degrees, *J. Biol. Chem. 132*, 57−64.
32. Felitsky, D. J., and Record, M. T. (2004) Application of the Local-Bulk Partitioning and Competitive Binding Models to Interpret Preferential Interactions of Glycine Betaine and Urea with Protein Surface, *Biochemistry 43*, 9276−9288.
33. Zhang, W. T., Capp, M. W., Bond, J. P., Anderson, C. F., and Record, M. T. (1996) Thermodynamic characterization of interactions of native bovine serum albumin with highly excluded (glycine betaine) and moderately accumulated (urea) solutes by a novel application of vapor pressure osmometry, *Biochemistry 35*, 10506−10516.
34. Hong, J., Capp, M. W., Anderson, C. F., and Record, M. T. (2003) Preferential interactions in aqueous solutions of urea and KCl, *Biophys. Chem. 105*, 517−532.
35. Courtenay, E. S., Capp, M. W., and Record, M. T. (2001) Thermodynamics of interactions of urea and guanidinium salts with protein surface: Relationship between solute effects on protein processes and changes in water-accessible surface area, *Protein Sci. 10*, 2485−2497.
36. Robinson, R. A., and Stokes, R. H. (1961) Activity coefficients in aqueous solutions of sucrose, mannitol and their mixtures at 25 degrees, *J. Phys. Chem. 65*, 1954−1958.
37. Bevington, P. R., and Robinson, D. K. (1992) *Data Reduction and Error Analysis for the Physical Sciences*, 2nd ed., WCB McGraw-Hill, Boston, MA.
38. Archer, D. G. (1992) Thermodynamic Properties of the NaCl+H2O System. 2. Thermodynamic Properties of NaCl(Aq), NaCl·2H2O-(Cr), and Phase-Equilibria, *J. Phys. Chem. Ref. Data 21*, 793−829.
39. Courtenay, E. S., Capp, M. W., Saecker, R. M., and Record, M. T. (2000) Thermodynamic analysis of interactions between denaturants and protein surface exposed on unfolding: Interpretation of urea and guanidinium chloride m-values and their correlation with changes in accessible surface area (ASA) using preferential interaction coefficients and the local-bulk domain model, *Proteins: Struct., Funct., Genet.*, 72−85.
40. Anderson, C. F., and Record, M. T. (1995) Salt Nucleic-Acid Interactions, *Annu. Rev. Phys. Chem. 46*, 657−700.
41. Anderson, C. F., Felitsky, D. J., Hong, J., and Record, M. T. (2002) Generalized derivation of an exact relationship linking different coefficients that characterize thermodynamic effects of preferential interactions, *Biophys. Chem. 101−102*, 497−511.
42. Anderson, C. F., Courtenay, E. S., and Record, M. T. (2002) Thermodynamic expressions relating different types of preferential interaction coefficients in solutions containing two solute components, *J. Phys. Chem. B 106*, 418−433.
43. Shi, Z. S., Woody, R. W., and Kallenbach, N. R. (2002) in *Advances in Protein Chemistry* (Rose, G. D., Ed.) pp 163−240, Academic Press, San Diego, CA.
44. Myers, J. K., Pace, C. N., and Scholtz, J. M. (1995) Denaturant *m* values and heat capacity changes: relation to changes in accessible surface areas of protein unfolding, *Protein Sci. 4*, 2138−2148.
45. Scholtz, J. M., Barrick, D., York, E. J., Stewart, J. M., and Baldwin, R. L. (1995) Urea Unfolding of Peptide Helices as a Model for Interpreting Protein Unfolding, *Proc. Natl. Acad. Sci. U.S.A. 92*, 185−189.
46. Smith, J. S., and Scholtz, J. M. (1996) Guanidine hydrochloride unfolding of peptide helices: Separation of denaturant and salt effects, *Biochemistry 35*, 7292−7297.
47. Spolar, R. S., Livingstone, J. R., and Record, M. T. (1992) Use of Liquid-Hydrocarbon and Amide Transfer Data to Estimate Contributions to Thermodynamic Functions of Protein Folding from the Removal of Nonpolar and Polar Surface from Water, *Biochemistry 31*, 3947−3955.
48. Spolar, R. S., and Record, M. T. (1994) Coupling of Local Folding to Site-Specific Binding of Proteins to DNA, *Science 263*, 777−784.
49. Creamer, T. P., Srinivasan, R., and Rose, G. D. (1995) Modeling unfolded states of peptides and proteins, *Biochemistry 34*, 16245−16250.
50. Auton, M., and Bolen, D. W. (2004) Additive transfer free energies of the Peptide backbone unit that are independent of the model compound and the choice of concentration scale, *Biochemistry 43*, 1329−1342.
51. Baskakov, I., and Bolen, D. W. (1998) Forcing thermodynamically unfolded proteins to fold, *J. Biol. Chem. 273*, 4831−4834.
52. Wang, A. J., and Bolen, D. W. (1997) A naturally occurring protective system in urea-rich cells: Mechanism of osmolyte protection of proteins against urea denaturation, *Biochemistry 36*, 9101−9108.
53. Burling, F. T., Weis, W. I., Flaherty, K. M., and Brunger, A. T. (1996) Direct observation of protein solvation and discrete disorder with experimental crystallographic phases, *Science 271*, 72−77.
54. Poole, P. L., and Barlow, D. J. (1986) The Relation of Ion-Pairs to Protein Hydration − an IR Spectroscopic and X-ray Crystallographic Survey, *Biopolymers 25*, 317−335.
55. Pettitt, B. M., Makarov, V. A., and Andrews, B. K. (1998) Protein hydration density: theory, simulations and crystallography, *Curr. Opin. Struct. Biol. 8*, 218−221.
56. Schneider, B., Patel, K., and Berman, H. M. (1998) Hydration of the phosphate group in double-helical DNA, *Biophys. J. 75*, 2422−2434.
57. Chalikian, T. V., Sarvazyan, A. P., Plum, G. E., and Breslauer, K. J. (1994) Influence of base composition, base sequence, and duplex structure on DNA hydration: apparent molar volumes and apparent molar adiabatic compressibilities of synthetic and natural DNA duplexes at 25 °C, *Biochemistry 33*, 2394−2401.
58. Ellerton, H. D., Reinfelds, G., Mulcahy, D. E., and Dunlop, P. J. (1964) Activity, density, and relative viscosity data for several amino acids, lactamide, and raffinose in aqueous solution at 25°, *J. Phys. Chem. 68*, 398−402.
59. Civera, M., Fornili, A., Sironi, M., and Fornili, S. L. (2003) Molecular dynamics simulation of aqueous solutions of glycine betaine, *Chem. Phys. Lett. 367*, 238−244.
60. Kiriukhin, M. Y., and Collins, K. D. (2002) Dynamic hydration numbers for biologically important ions, *Biophys. Chem. 99*, 155−168.
61. Robinson, R. A., and Stokes, R. H. (1959) *Electrolyte solutions*, 2nd ed., Butterworth Scientific Publications, London.
62. Lindenbaum, S., and Boyd, G. E. (1964) Osmotic and activity coefficients for the symmetrical tetraalkylammonium halides in aqueous solutions at 25°, *J. Phys. Chem. 68*, 911−917.
63. Levien, B. J. (1965) Some physical properties of aqueous solutions of tetramethylammonium bromide and tetramethylammonium iodide, *Austrian J. Chem. 18*, 1161−1170.
64. Saecker, R. M., and Record, M. T., Jr. (2002) Protein surface salt bridges and paths for DNA wrapping, *Curr. Opin. Struct. Biol. 12*, 311−319.
65. Hong, J., Capp, M. W., Anderson, C. F., Soecker, R. M., Felitsky, D. J., Anderson, M. W., and Record, M. T., Jr. (2004) Preferential Interactions of Glycine Betaine and of Urea with DNA: Implications for DNA Hydration and for Effects of These Solutes on DNA Stability, *Biochemistry 43*, 14744−14758.

BI049115W